


Combined Delivery of Two Different Bioactive Factors Incorporated in Hydroxyapatite Microcarrier for Bone Regeneration

Tae-Woo Kim¹ · Woo-Beom Ahn¹ · Joong-Min Kim^{1,2} · Joong-Hyun Kim^{3,4,5} · Tae-Hyun Kim^{4,5} · Roman A. Perez^{4,5,6} · Hyon-Seok Jang¹ 

Received: 9 February 2020 / Revised: 3 March 2020 / Accepted: 24 March 2020 / Published online: 16 August 2020
© The Korean Tissue Engineering and Regenerative Medicine Society 2020

Abstract

BACKGROUND: The delivery of growth factors using a carrier system presents a promising and innovative tool in tissue engineering and dentistry today. Two of the foremost bioactive factors, bone morphogenetic protein-2 and vascular endothelial growth factor (VEGF), are widely applied using a ceramic scaffold. The aim of this study was to determine the use of hydroxyapatite microcarrier (MC) for dual delivery of osteogenic and angiogenic factors to accelerate hard tissue regeneration during the regenerative process.

METHODS: Two MCs of different sizes were fabricated by emulsification of gelatin and alpha-tricalcium phosphate (α -TCP). The experimental group was divided based on the combination of MC size and growth factors. For investigating the *in vitro* properties, rat mesenchymal stem cells (rMSCs) were harvested from bone marrow of the femur and tibia. For *in vivo* experiments, MC with/without growth factors was applied into the standardized, 5-mm diameter defects, which were made bilaterally on the parietal bone of the rat. The animals were allowed to heal for 8 weeks, and samples were harvested and analyzed by micro-computed tomography and histology.

RESULTS: Improved proliferation of rat mesenchymal stem cells was observed with VEGF loaded MC. For osteogenic differentiation, dual growth factors delivered by MC showed higher osteogenic gene expression, alkaline phosphatase production and calcium deposition. The *in vivo* results revealed statistically significant increase in new bone formation

Tae-Woo Kim and Woo-Beom Ahn contributed equally to this work as first authors.

Electronic supplementary material The online version of this article (<https://doi.org/10.1007/s13770-020-00257-5>) contains supplementary material, which is available to authorized users.

✉ Hyon-Seok Jang
omfs119@korea.ac.kr

¹ Department of Dentistry, Graduate School of Medicine, Korea University, 73 Goryeodae-ro, Seongbuk-gu, Seoul 02841, Republic of Korea

² e-Well Dental Hospital, Suite #214, Daebang B/D, Shindaebang-dong, Dongjak-gu, Seoul 07056, Republic of Korea

³ Laboratory Animal Center, Osong Medical Innovation Foundation, 123 Osongsangmyeong-ro, Osong-eup, Heungdeok-gu, Cheonju-si, Chungbuk 28160, Republic of Korea

⁴ Institute of Tissue Regeneration Engineering (ITREN), Dankook University, 119 Dandae-ro, Dongnam-gu, Cheonan-si, Chungnam 31116, Republic of Korea

⁵ Department of Nanobiomedical Science, BK21 PLUS NBM Global Research Center for Regenerative Medicine, Dankook University, 119 Dandae-ro, Dongnam-gu, Cheonan-si, Chungnam 31116, Republic of Korea

⁶ UIC Regenerative Medicine Research Institute, Universitat Internacional de Catalunya, Carrer de la Immaculada 22, 08017 Barcelona, Spain

when dual growth factors were delivered by MC. Dual growth factors administered on a calcium phosphate matrix showed significantly enhanced osteogenic potential.

CONCLUSION: We propose this system has potential clinical utility in providing solutions for craniofacial bone defects, with the added benefit of early availability.

Keywords Drug carriers · BMP-2 · VEGF · Drug delivery system · Bone regeneration

1 Introduction

Research is ongoing to study the effects of growth factors incorporated with biomaterials and applied to the human body to promote new bone formation [1]. Biomaterials with excellent osteogenesis and angiogenesis are desirable for the treatment of massive bone defects caused by trauma, tumors, infections or genetic malformations [2]. During the bone repair process, osteogenesis and angiogenesis are closely associated, and a well-coordinated transient angiogenic response is crucial for successful bone repair [3]. When new angiogenesis occurs, the transfer of nutrients, oxygen, calcium, and phosphate to the bone defect site is increased, and the mesenchymal stem cells are transported to promote bone regeneration [4]. The development of synthetic biomaterials coupling osteogenesis and angiogenesis has attracted increasing attention in recent years [2]. Local administration of growth factors utilizing various polymeric and ceramic biomaterials has therefore pointedly been investigated for sustained drug delivery [5]. However, synthetic polymers have the disadvantage of inducing an inflammatory response during *in vivo* degradation, and it is difficult to achieve a uniform distribution and sustainable release of water-insoluble drugs. Ceramics are inorganic biomaterials that are used as bone replacements due to their high compressive strength, biodegradability and osteoconductivity [5]. However, ceramics have the disadvantage that they lack an intrinsic mechanism for controlled delivery and are difficult to mold into the desired defect geometry. Thus, the development of biomaterials that are more biocompatible and capable of controlling biodegradability remains a challenge for the sustained delivery of growth factors.

Hydroxyapatite (HA) is widely used as a synthetic bone graft material for periodontal and dental implant surgery, and has added advantages of bioactivity and osteoconductivity [6, 7]. The bone substitute used in the present study is HA fabricated by the calcium phosphate cement paste (CPC) emulsion method. Various sized microporous microcarriers (MCs) were prepared using alpha-tricalcium phosphate (α -TCP) with gelatin slurries at low temperature by a water-in-oil emulsion, taking advantage of the setting reaction of a CPC. The osteoinductive potential and properties that allow osteoconduction into bone defect area has resulted in the wide application of HA-MCs in tissue

engineering [8]. In addition, their sphericity results in better filling and maintaining irregular defect space for new bone formation, and also provides a high surface area to cells, enabling high yield culturing and *in vivo* delivery of adherent cell types [9]. However, since the osteogenic effect of MC is weaker than the autologous bone, bone regeneration takes a long time for complete recovery in the presence of such synthetic materials [6]. To overcome some of the disadvantages and improve bone graft efficiency, osteoconductive MC can be combined with mesenchymal stem cells (MSCs) and/or osteogenic and angiogenic growth factors such as bone morphogenetic proteins (BMPs) and vascular endothelial growth factors (VEGFs). The delivery of bone matrix and cell or growth factor complex can be applied more effectively in new bone formation than the autologous grafts, which are regarded as the gold standards for bone substitutes. The MC developed by Dr. Perez has micropores on the surface that serve as nucleation sites for biological apatite precipitation, and macropores that provide potential spaces for new bone maturation and possible sites for entrapment of growth factors [6].

A group of secreted proteins that belong to the transforming growth factor- β (TGF- β) superfamily, BMPs have been widely used to induce increased cartilage and bone formation [10]. BMPs appear to improve initiation of cartilage and bone formation by two different pathways, namely, osteogenesis and angiogenesis [10]. Among the BMP family members, BMP-2 induces the osteoblastic differentiation *in vitro* and improves osteoinductive activity *in vivo* [10]. Moreover, BMP-2 is commonly used in clinical conditions to effectively induce osteogenesis [11]. Although BMP-2 is an important osteogenic factor for inducing bone formation, bone regeneration is a highly complicated process involving various other growth factors [10]. VEGF is the most well characterized angiogenic factor, and is responsible for bone healing and skeletal formation. BMP-2 enhances bone formation in the coupling of angiogenesis through up-regulation of gene expression of VEGF in osteoblast-like cells. In addition, VEGF induces BMP-2 expression and indirectly stimulates osteoblast differentiation. Even on their own, both BMP-2 and VEGF are involved in bone formation. However, it has been proposed that the combined administration of BMP-2 and VEGF can obtain more effective bone regeneration as

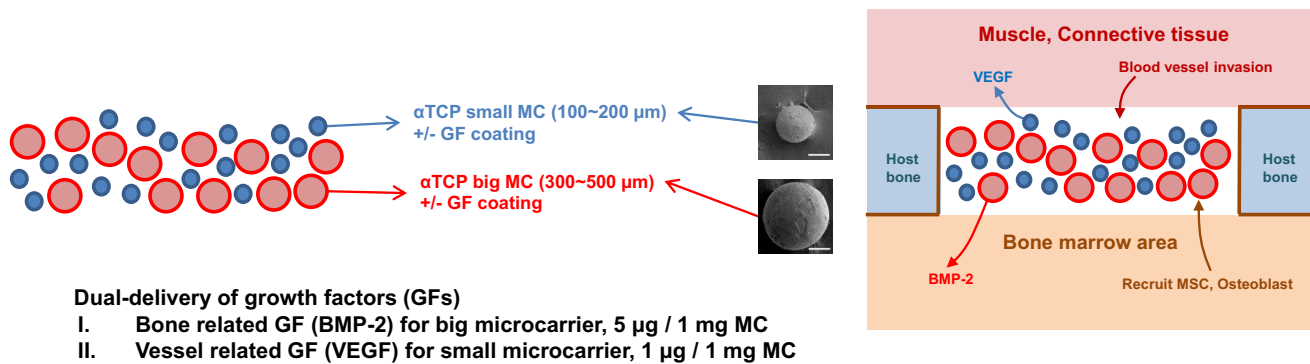


Fig. 1 Schematic plane of the application with two bioactive factors incorporated in the α -TCP microcarrier (magnification $\times 200$, scale bar = 100 μm) for bone regeneration

compared with single use [10]. Hence, more attention has been focused in combining osteogenic and angiogenic effects to promote bone regeneration.

Although a supraphysiologic dose of growth factor is usually applied to effectively induce tissue regeneration in clinical situations, it is necessary to administer the growth factor at a lower dose to prevent possible adverse effects [7, 11]. Studies have applied osteoconductive matrix for surgical defects in animal models containing growth factors lower than the clinical dose [7]. Coating the grafts with growth factor is found to be more effective than moistening with diluted growth factor, thereby preventing incorrect dosing and uncontrolled flow [12, 13]. This study was therefore undertaken to investigate the potential of an HA-MC based on α -TCP coated with two different growth factors, and to evaluate the suitability of this carrier system for possible clinical applications in bone tissue engineering. The mean size of MC and study scheme is summarized in Fig. 1. In order to elucidate the efficacy of the combination of two growth factors with two different sized MCs, *in vitro* studies on rat bone marrow-derived (rMSCs) were performed, and critical sized rat calvarial defect model was included to assess *in vivo* bone regeneration.

2 Materials and methods

2.1 Fabrication of calcium phosphate microcarrier

To generate MCs, powders of the relevant CPC were obtained from the appropriate mixture of calcium hydrogen phosphate (CaHPO_4 , C7263, Sigma-Aldrich, Atlanta, GA, USA) and calcium carbonate (CaCO_3 , C4830, Sigma-Aldrich) by sintering at 1400 $^\circ\text{C}$ and subsequent quenching. The obtained α -TCP was treated with a planetary mill (Pulverisette 6, Fritsch GmbH, Idar-Oberstein, Germany), and a 2 wt% of precipitated HA (ref.1.02143, Merck-KgaA, Darmstadt, Germany) was included as the seed of

the precipitation reaction in the obtained powder. To obtain a gelatin/calcium phosphate composite paste, the complete inorganic powder prepared in the previous step was mixed with a gelatin solution at 5% (w/vol) by adjusting the ratio of liquid to powder at 0.8 mL/g. The ceramic slurry was added into heated olive oil with stirring, until setting time was reached. Once the microspheres were formed, the MCs were extracted by adding an ice-cold washing solution into the oil emulsion. After cross-linking with 1.15% (w/v) 1-ethyl-3,3-(3-dimethylaminopropyl) carbodiimide (EDC; Fluka 39,391, Sigma-Aldrich) and 0.03 M N-hydroxysuccinimide (13,067-2, Sigma-Aldrich) for 2 h, the supernatant was discarded and the MCs were separated, cleaned with acetone, and immersed in Ringers solution for 7 days for α -TCP hydrolysis, to enable the complete transformation into HA.

2.2 Diameter and porosity of microcarrier

The MCs obtained were sieved, and MCs in the diameter range of 100–200 μm (small, S) and 300–500 μm (big, B) were selected for this study. The size of each MC was scanned using high resolution scanning electron microscopy (SEM; JEOL-JSM 6510, Tokyo, Japan) to observe the external and internal structure. SEM images of MC were taken randomly from each sample at 200X magnification, and the diameters were measured for each image. The porosity was evaluated by performing micro-computed tomography (μCT , skyscan 1176, SkyScan, Aartselaar, Belgium). Micro-CT images scanned at a resolution of 18 μm (65 kV and 378 μA), and the region of interest (ROI) was reconstructed from the scanned data set. Porosity of the each MC was measured with a μCT analyzer program (CTAn, SkyScan), and the coronally sectioned two dimensional (2D)-reconstructed image was visualized using a data viewer program (SkyScan).

2.3 Growth factor release profile

Prior to the experiment and growth factor loading, the collected MCs were sterilized by immersing in 70% ethanol and placed under a UV lamp for 4 h. The sterile MCs were then washed three times by sterile PBS. Prepared MCs were incubated with PBS overnight before loading with BMP-2 (Cowell Medi Implant, Busan, Korea) and VEGF (R&D systems, Minneapolis, MN, USA). Growth factor loaded MCs were maintained in a freezer until use; the day before use, frozen MCs were lyophilized and used for the release test. The MCs (quadruplicate samples from each batch) were suspended in 1 ml PBS, and were gently shaken in a humidified incubator at 37 °C. At defined time intervals, all PBS was collected without removing MCs and replaced with fresh PBS. The collected supernatants were stored frozen at – 80 °C until the end of the experiment, and were then assayed for growth factor content using the human VEGF 165 (900-K10) and the human BMP-2 (900-K255) enzyme-linked immunosorbent assay (ELISA) kit, obtained from Peprotech Inc. (Peprotech, Rocky Hill, NJ, USA).

2.4 Harvest and characterization of bone marrow derived MSC from rat long bone

Animal cell primary culture was performed after receiving approval from Korea University, Institutional Animal Care and Use Committee, Republic of Korea. Using an explant technique, the bone marrow derived rat mesenchymal stem cells (rMSCs) were harvested from 5-week-old male Sprague-Dawley (SD) rats (Daehan Biolink, Chungbuk, Republic of Korea). Briefly, the rats were sacrificed, and the tibia and femur from both legs were separated and soft tissues were removed. Both ends of each bone were snipped, and the bone marrow area was washed twice with media, and digested with collagenase type I and dispase solution. rMSCs were cultured in controlled medium consisting of α -modified minimal essential medium (α -MEM, SH30265.02, HyClone, Logan, UT, USA) supplemented with 10% fetal bovine serum (FBS, SH30919.03, HyClone), and 100 U/ml penicillin and 100 mg/ml streptomycin (Pen/Strep, 15,140-122, Gibco, Carlsbad, CA, USA), at 37 °C in a humidified atmosphere containing 5% (v/v) CO₂. As opposed to hematopoietic cells, MSCs adhere to the surface of the culture dish; twice a week, the adherent cells were separated from the bone marrow by adherence-separation culturing and replacing the culture medium. For passaging, upon reaching 80% confluence, cells were gathered by trypsinization (0.05% (w/v) trypsin-EDTA, 25,300-062, Gibco), and re-plated in a new culture dish. Fresh medium was replenished every 3 days, and the

cells between passages 3 and 4 were used for the experiments.

Before use, expression levels of the surface-antigen markers on the isolated bone marrow-derived rMSCs were confirmed by fluorescence-activated cell sorting (FACS) analysis (FACSCalibur, BD Biosciences, San Jose, CA, USA). Some characteristic surface markers for multipotent mesenchymal stem cells analyzed were as follows: positive for CD44 (sc7946, Santa Cruz Biotechnology Inc., Paso Robles, CA, USA), CD73 (sc14682), CD105 (sc19793), CD106 (sc8304), CD146 (ab75769, Abcam, Cambridge, MA, USA), runt-related transcription factor 2 (RUNX2, sc10758) and transforming growth factor- β receptor 1 (TGF- β R1, ab31013), and negative for CD31 (sc1506) and CD34 (sc7045). Briefly, rMSCs were washed with cold PBS, fixed in 4% paraformaldehyde (PFA), and stained with primary antibodies of each factor. FITC-labeled secondary antibodies were also added, and the samples were analyzed by FACS.

2.5 Cell proliferation

The direct effect of MCs and the indirect effect of the released growth factors on cell proliferation were evaluated *in vitro*. For the direct proliferation test, 5×10^4 rMSCs were seeded onto each sample. At each time point, the DNA content of the samples was evaluated through DNA quantification using double-stranded DNA (dsDNA) fluorescence kit (PicoGreen quantitation assay kit, P11496, Invitrogen, Carlsbad, CA, USA), according to the manufacturer's instructions. Briefly, the cultured cells were lysed, followed by three freeze/thaw cycles using 0.2% triton solution. Cell lysates were centrifuged at 12,000 rpm at 4 °C for 15 min, and the resultant supernatants were analyzed. PicoGreen reagent and samples were mixed in equal volumes (50 μ l each) and incubated for 5 min in the dark. Three samples in each group were measured using a multimode microplate plate reader (SpectraMax M2e, Molecular Devices Corporation, Sunnyvale, CA, USA), and the data were averaged from duplicate tests. A standard curve was generated using the provided dsDNA standard sample, and the intensity of the experimental samples was interpolated to determine the cell attachment and proliferation of the rMSCs. For the indirect proliferation assay, 6×10^3 rMSCs were seeded on the culture plates, and the cell proliferation level was quantified by cell counting kit-8 (CCK-8, Dojindo Molecular Technologies, Inc., Kumamoto, Japan). Briefly, cells were cultured for 1, 3, 5, 7, and 9 days, after which the plates were washed twice with PBS, and culture media containing 10% CCK-8 reagent was added to each well. After 2 h incubation at 37 °C, 100 μ l aliquots from each well were transferred to a 96-well plate,

and the proliferative activity was determined spectrophotometrically at 450 nm using a microplate reader.

2.6 Osteogenic differentiation

The osteogenic performance of MC and growth factor loaded MC was compared in 3 replicates for each group. rMSCs were seeded at a density of $4 \times 10^4/\text{cm}^2$; cells were then differentiated in osteogenic medium, with media changes every 3 days. For osteogenic differentiation, controlled medium was supplemented with 10 mM β -glycerophosphate (G9422, Sigma-Aldrich), 50 $\mu\text{g}/\text{mL}$ ascorbic acid (A8960, Sigma-Aldrich), and 100 nM dexamethasone (D4902, Sigma-Aldrich). In order to visualize the overall cell distribution and mineralization of rMSCs on the samples, SEM images were obtained. Briefly, the cells grown in each sample were fixed by 4% PFA, dehydrated in a graded series of ethanol (70, 80, 90, 95 and 100%), treated with hexamethyldisilazane to complete dehydration of the samples, followed by air-drying of the samples. The types of ECM(extracellular matrix) formation and cell distribution were confirmed after carbon coating. In order to assess the *in vitro* efficiency of the MCs on the osteogenic differentiation on the rMSCs, two sets of experiments were performed. Indirect culturing was done to verify mineral deposition, and alkaline phosphatase (ALP), total protein, and gene expression changes were evaluated for the direct culture studies.

2.7 Quantitative reverse transcription-polymerase chain reaction (qPCR) analysis

After the cells were exposed to the different growth factor conditions, the gene expression of *ALP*, osteocalcin (*OCN*) and osteopontin (*OPN*) in the rMSCs were detected by a quantitative real-time PCR (qRT-PCR) using specific primer sequences for the listed genes (Table 1). The rMSCs were collected at 10 days from each study group described

Table 1 Primer sequences for quantitative real time-PCR

Target gene	Direction	Primer sequence
<i>GAPDH</i>	Forward	GGCAAGTTCAACGGCACAGT
	Reverse	CGCTCCTGGAAGATGGTGAT
<i>ALP</i>	Forward	ACTGGTACTCGGACAATGAG
	Reverse	ATCGATGTCCTTGATGTTGT
<i>OPN</i>	Forward	CCAAGCAACTCCAATGAAAGC
	Reverse	TCCTCGCTCTCTGCATGGT
<i>OCN</i>	Forward	CAGACAAGTCCCACACAGCAA
	Reverse	GCCAGCAGAGTGAGCAGAGA

previously, with untreated cells as a control. To analyze expression of genes involved in MSC osteogenic differentiation, the total cellular RNA was extracted using the RNeasy Minikit (74,106, Qiagen, Gaithersburg, MD, USA) from each cell sample, and the cDNA was synthesized from the total RNA. qRT-PCR was performed by using real-time PCR equipment (StepOnePlus™, Applied Biosystems, Waltham, MA, USA) and SensiMix™ SYBR Kit (QT605, Bioline, London, UK).

2.8 Mineralized nodule formation by alizarin red S staining and cetylpyridinium chloride quantification

To demonstrate the presence of insoluble calcium deposition, the differentiated cells were assayed at days 5, 10, 15 and 20. Briefly, at the prescribed time points, the samples were fixed in 70% ice cold ethanol for 1 h and rinsed with distilled water. Cells were stained with 40 mM Alizarin Red S (ARS, A5533, Sigma-Aldrich) solution (pH 4.2) at room temperature for 10 min, with gentle agitation. Cells were then gently rinsed with distilled water to remove any unbounded dye. The ARS staining was photographed under stereo microscope (JSZ-7XT; Samwon Scientific, Seoul, Republic of Korea). For quantification of staining, ARS was extracted with 10% (w/v) cetylpyridinium chloride (CPC, C0732, Sigma-Aldrich) for 30 min at room temperature with gentle shaking. After incubation, aliquots of the ARS extracts were transferred to a 96-well plate, and the concentration was determined spectrophotometrically at 562 nm, in triplicate.

2.9 Determination of alkaline phosphatase activity

The enzymatic activity of ALP was determined by a colorimetric assay to check osteogenic differentiation of rMSCs at days 7, 14 and 21, subsequent to cell seeding under osteogenic culture conditions (control, SV, BB, SVBB). The MCs were washed twice with PBS, and the cell lysates were obtained from each sample. The cells were lysed thrice by freeze–thaw cycles, followed by addition of 0.2% triton. The sample lysates were collected in tubes and centrifuged at 10,000 rpm for 10 min. The cell supernatants were assessed for ALP activities using the ALP detection reagent containing p-nitrophenyl phosphate (p-NPP) as the substrate. Working reagent containing equal parts (1:1:1) of 1.5 M 2-amino-2 methyl-1-propanol (A5888, Sigma-Aldrich), 20 mM p-NPP (P4744, Sigma-Aldrich), and 1 mM magnesium chloride (208,337, Sigma-Aldrich) were added to the samples, and incubated at 37 °C. The reaction was terminated by transferring sample tubes on ice and adding the stop solution. The absorbance of the resultant p-nitrophenol was quantified using a

microplate-reader (iMark, BioRad, CA, US) at a wavelength of 405 nm, and the concentration was calculated from a standard ALP activity curve generated using p-nitrophenol stock standard (N7660, Sigma-Aldrich). The produced ALP was normalized by dsDNA produced from each sample, and the ALP specific activity was calculated. Each test was performed on four replicate samples ($n = 4$).

2.10 Animals and *in vivo* design

The protocol of housing, care and experimental procedure were approved by the Korea University, Institutional Animal Care and Use Committee, Republic of Korea; the animal selection, management, surgical protocol, and preparation was as per the procedure of our previous study [14]. A total of 27 animals, 12 weeks old, 250–300 g healthy male SD rats were included in this study. Upon arrival, the animals were housed individually, and allowed to acclimate for a week. The standard pellet food and water were provided *ad libitum*. The first subcutaneous animal model was used to determine tissue reactions of the cell/scaffold tissue-engineered samples (small size MC (S), big size MC (B), small and big size MC (SB), small size MC with VEGF (SV), big size MC with BMP-s (BB), SV with BB (SVBB) groups). Next, the critical sized calvarial bone defect model (5 mm in diameter) was designed to investigate the regeneration of bone tissues by the dual growth factor induced MCs. The experimental groups included one study group (SVBB) and two control groups (SB and empty control).

2.11 Surgical procedure

All surgical procedures were performed under general anesthesia, induced with a mixture of 80 mg/kg ketamine hydrochloride (Ketamine®, Yuhan, Seoul, Korea) and 10 mg/kg xylazine (Rumpun®, Bayer Korea, Seoul, Korea) administered via an intramuscular injection. After anesthetizing the animals, the back of each rat was shaved and the surgical site was scrubbed with 10% povidone iodine and 70% ethanol in a standard manner. A single 1.5 cm incision was made through the skin on the midline, and four subcutaneous pouches were created using blunt dissection laterally on the rear. A single randomized specimen was placed in each pouch, away from the incision. Following implantation, the incision was subsequently sutured with 4–0 non-absorbable monofilament suture material (Prolene, Ethicon, Somerville, NJ, USA). The animals were sacrificed at 8 weeks after the surgery.

For the calvarial defect model, the animals were anesthetized by injecting ketamine and xylazine mixture during the surgical procedure. After the surgical site was prepared, infiltration anesthesia with 0.5% lidocaine (with 1:100,000

epinephrine) was administered to the surgical sites over the calvarial bone to decrease the pain and bleeding during operation. The animals were placed in ventral recumbency, and their heads were shaved. The operation field was then prepared for aseptic surgery, using 10% povidone iodine and 70% ethanol serially. After a straight incision along the sagittal midline of the skin, a full thickness flap (including the skin and the periosteum) was elevated, and the underlying parietal bone was exposed. A 5 mm diameter trephine bur was used to create a standardized, and bilateral full-thickness round defect in each parietal bone. During the creation of the defect, the surgical field was continuously irrigated with cold sterile 0.9% saline, and the trephined bony disk was carefully removed. After this treatment, the experimental and control materials were appropriately applied to the defect; the defects were left empty in the ‘empty control’ group. After delivery of the grafting material, the periosteum was repositioned and sutured with 4–0 absorbable suture material (Vicryl, Ethicon), and the skin was sutured with 4–0 non-absorbable suture materials. Post surgery, the animals were monitored for signs of infection, inflammation and adverse effects by visual observation, and the suture was removed after 7 days. After a healing period of 8 weeks, the animals were sacrificed by CO₂ inhalation and cervical dislocation, and the samples and surrounding tissues were harvested for analysis.

2.12 Image analysis of Micro-CT

After obtaining block sections, including the defect and the surrounding bone, each block section was fixed in 10% neutralized buffered formalin for 24 h, and then transferred to 70% ethanol until scanning. The samples were scanned using an *in vivo* high resolution μ CT (SkyScan 1176, SkyScan) at a resolution of 18 μ m (100 kV and 100 μ A) with a filter of 1 mm aluminum. The scanned data set were reconstructed in the reconstruction software (NRecon, Skyscan), and the volume of interest (VOI) was positioned over each defect on the serial coronally sectioned images for quantitative analyses. For quantitative analyses of encompassing the new bone within the defect site, three-dimensional (3D) images were created using an image analyzer program (CTAn Skyscan) by reconstructing images over the VOIs and analyzing for the percentage new bone volume, the bone surface area, and the bone surface density.

2.13 Histologic analysis

After μ CT imaging, the fixed samples were decalcified in RapidCal™ solution (BBC Chemical, Stanwood, WA, USA), followed by dehydration in a graded series of

increasing ethanol dilutions (from 70 to 100%). All samples were bisected in the middle of the defect and embedded in paraffin to make blocks. Using a microtome (RM2245, Leica, Germany), 5 μm thick sections were cut into the sagittal plane along the center of the defect in each block. The most-central sections were placed on glass slides and stained with hematoxylin and eosin (H&E), using a standard techniques. The slides were then observed under a light microscope (IX70, Olympus Co., Tokyo, Japan) to assess biocompatibility and tissue regeneration, and digital images were photographed using Meta-Morph (Universal Imaging Corporation, Downingtown, PA, USA).

2.14 Statistical analysis

Experiments were run in triplicate to account for individual variations. Statistical analyses were performed using SPSS. The one-way analysis of variance (ANOVA) test was performed to determine significant differences between

groups. The level of statistical significance was set at $p < 0.05$, and the values are reported as mean \pm standard deviation of the mean of three independent experiments.

3 Results

3.1 Microcarrier formation and characterization

HA-MCs of varying sizes were fabricated by a combination of α -TCP and gelatin emulsification, using the water-in-oil emulsion method. During the process, MCs having an average particle size in the range of 100–500 μm were obtained. The MCs possessing diameters of 100–200 μm (small size, S) and 300–500 μm (big size, B) were collected for further experiments. The MCs observed with optical microscopy are shown in Fig. 1. No macroscopic morphological differences were observed between MCs of different particle size. Figure 2 shows the morphology of the MC and their size distribution by SEM. Each MC has a

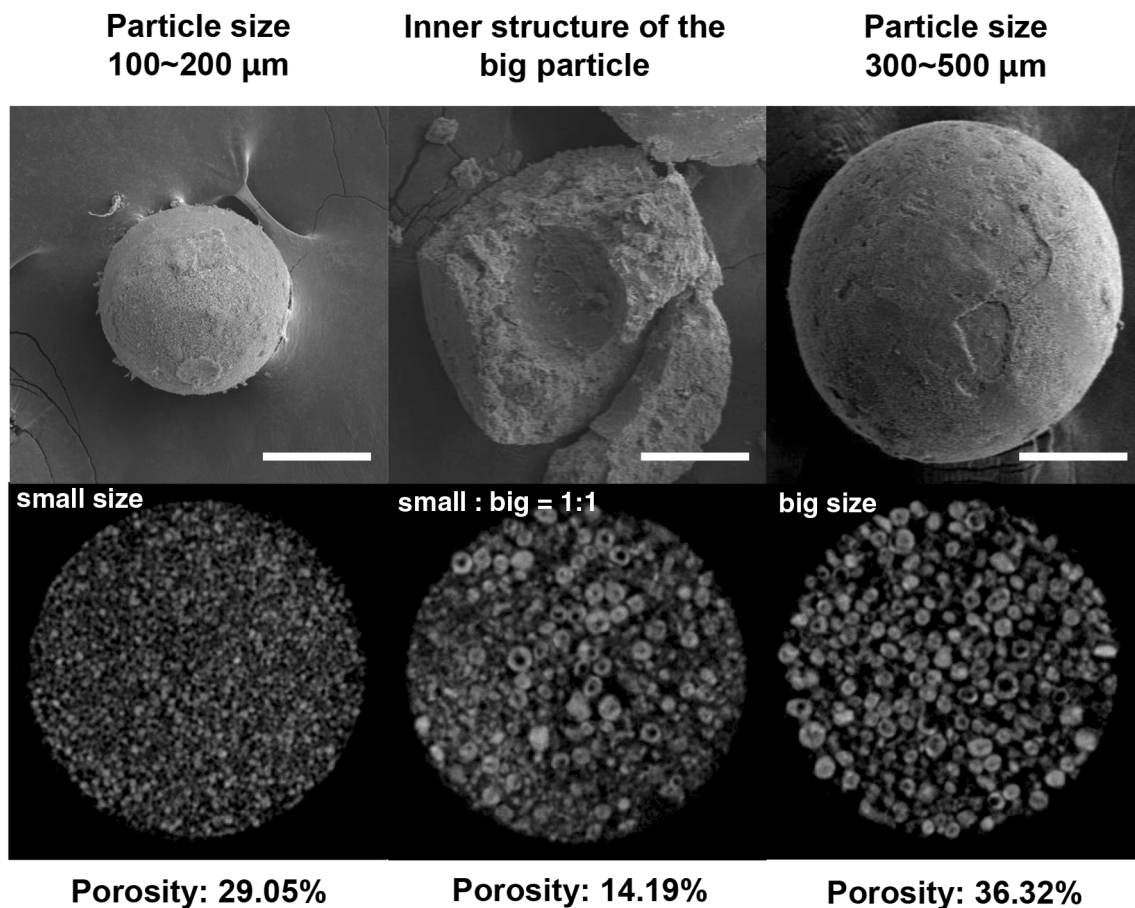


Fig. 2 SEM micrographs of HA-MC (magnification $\times 200$, scale bar = 100 μm). Two resultant MCs of small (100–200 μm), and big (300–500 μm) size with hollow internal structure are shown. No surface morphological differences were observed between the MCs.

μCT images of MCs, and the porosity calculated from μCT data analysis are also presented. *SEM* scanning electron microscopy, *HA* hydroxyapatite, *MC* microcarrier, *μCT* : micro-computed tomography

similar outer and hollow internal structure. The calculated porosity of each MC is also presented. Three dimensional μ CT images were defined by scanned images, and the porosity of the MCs were assessed using μ CT image analysis program as described in the Materials and Methods section. Big MCs had a higher porosity (36.32%) compared to the small MCs (29.05%). When two sizes of MCs were mixed in a 1:1 ratio (SB), the resultant porosity was 14.19%.

3.2 Accumulated concentration of released protein

The *in vitro* release profile of VEGF from the small size MC (SV), BMP-2 from big size MC (BB), and dual growth factor loaded MCs (SVBB), were examined by an ELISA quantification assay. Figure 3A and B show the accumulative amount of growth factors released from the MCs. After a rapid burst release (within few hours), the growth factors retained a sustained release profile, which continued up to 21 days. The incremental release curve re-plotted in Fig. 3C and D further demonstrates the release behavior in

a time-dependent manner. The total release amount was approximately 728.9 ng (corresponding to 72.9% of the incorporated VEGF) from SV and 2580.2 ng (corresponding to 51.6% of the incorporated BMP-2) from BB. The total release amount from SVBB was approximately 536.8 ng (corresponding to 53.7% of the incorporated VEGF) and 1945.6 ng (corresponding to 38.9% of the incorporated BMP-2) (Fig. 4).

3.3 Stem cell characterization and their growth on MCs

Prior to determining the effect of dual growth factor incorporated MCs on the rMCSs, some representative surface markers of multipotent MSCs were evaluated using FACS analysis. The rMCSs expressed typical marker pattern for MSCs: high levels of positive signals for TGF- β 1 (99.25%), RUNX2 (99.16%) CD44 (99.50%), CD73 (99.59%), CD105 (99.28%) CD106 (99.18%), and CD146 (99.18%), and low levels of negative signals for CD31 (3.36%) and CD34 (2.34%). These results indicate that the

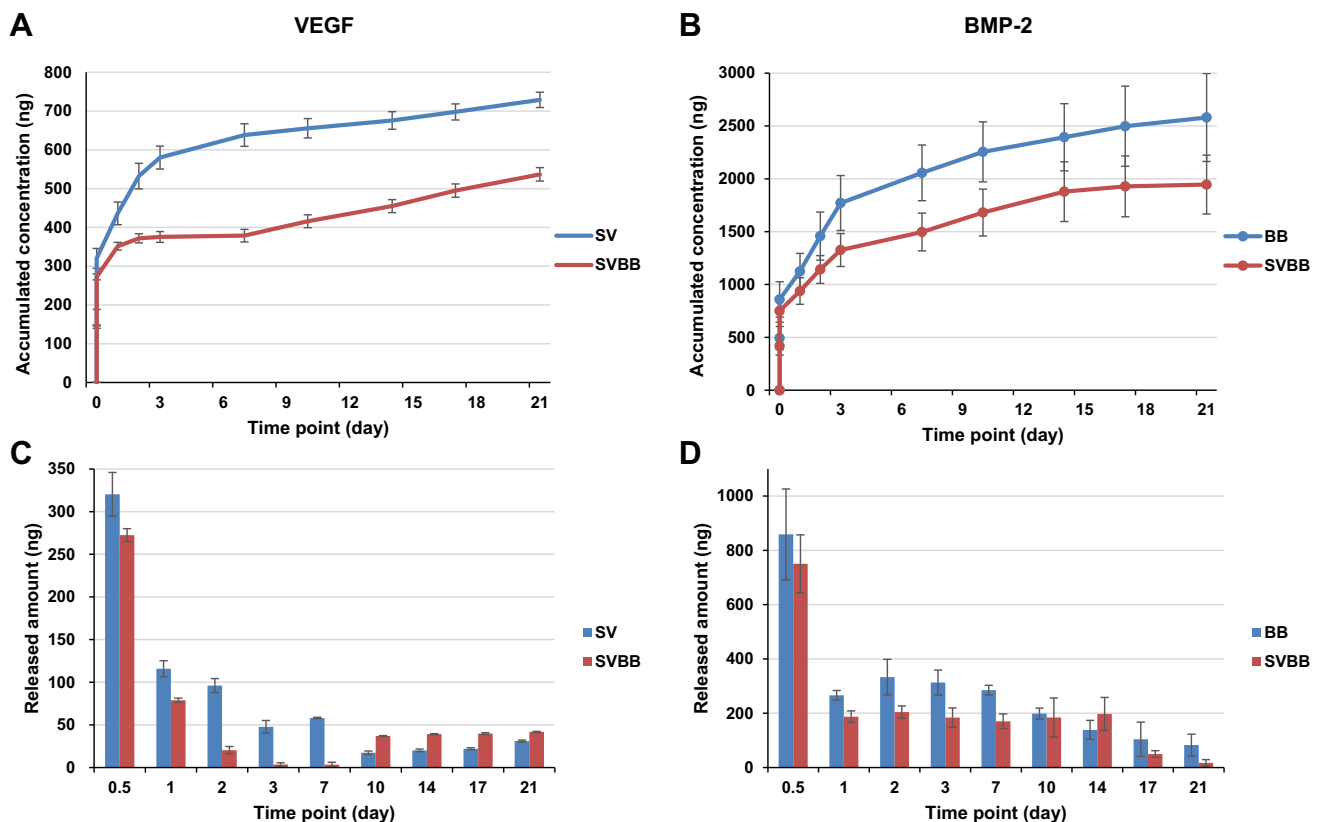


Fig. 3 A–D *In vitro* growth factor release profile of VEGF and BMP-2. **A** Accumulative release profiles and **C** released dosage profiles from MCs containing VEGF with small size MC and **B** accumulative release profiles and **D** released dosage profiles from MCs containing BMP-2 with big size MC. Release profiles indicate a rapid burst release (within few hours) of growth factor from MCs. Both single

and dual growth factor loaded MCs showed a sustained release profile that continued up to day 21. This indicates the possibility of regulating the amount of release of two growth factors in one type of MCs. SV: small size microcarrier with VEGF; SVBB: mixed microcarrier with BMP-2 and VEGF; BB: big size microcarrier with BMP-2

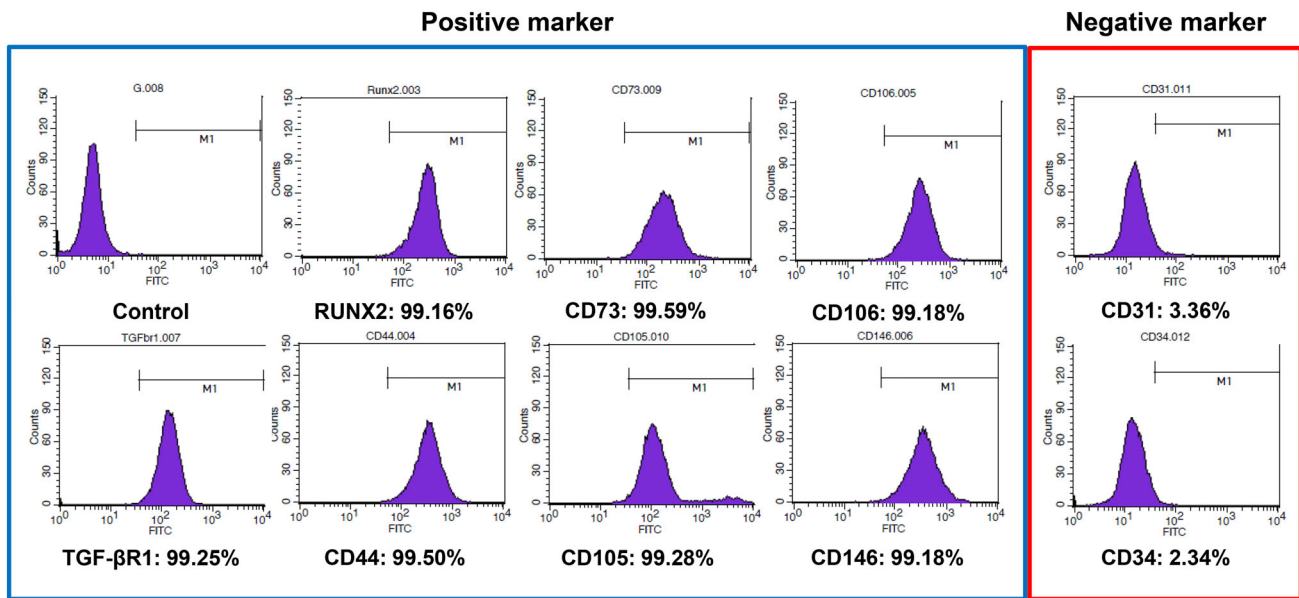


Fig. 4 FACS analysis of surface antigen expression of rMSCs. rMSCs stained positive for TGF- β R1, RUNX2, CD44, CD73, CD105, CD106, and CD146, and negative for CD31 and CD34. rMSCs: rat

bone marrow-derived mesenchymal stromal cells. TGF- β R1: transforming growth factor- β receptor 1, Runx2: runt-related transcription factor 2

primary cultured rMSCs used in this study possess characteristics of multipotency.

To investigate the effect on cell proliferation with MC, dsDNA was quantified for rMSCs up to 21 days (Fig. 5A). In the direct culture assay, we observed the amount of dsDNA of rMSCs at day 7 was higher in the SV group as compared to other groups. The SV and BB exposed cells also grew faster than the control group. The proliferation of cells exposed to SVBB increased more rapidly at 7 days, but was different at days 14 and 21. The highest increase of dsDNA amount was observed in SV at days 14 and 21, compared to other groups. There was no significant difference in the proliferation of rMSCs between BB and SVBB, and both showed significantly higher dsDNA amount than the control group during the study period. The differences between groups seemed to be more pronounced in the indirect culture test. The cells cultured with the released growth factors grew without reaching a plateau on day 9 (Fig. 5B). There was no difference between the groups until day 5, but the number of cells tended to increase statistically in SV after 7 days ($P > 0.05$). Figure 5C shows the contrast microscopy images obtained for cell culture under indirect culture conditions.

3.4 Cell differentiation and ECM deposition on the MCs

The shape of the ECM deposition on MC after osteogenic differentiation is presented in Fig. 6. At low magnifications, integration between HA-MCs by ECM can be

observed after differentiation by SEM. The MCs were intact, and no fragments were detached from the MC. Despite the qualitative nature of the images, incorporating VEGF with MC resulted in increased ECM formation than MC with BMP-2. Cells tended to proliferate at the interface between the different MCs, and were aggregated.

3.5 Gene expression of rMSCs on the MCs

Since different growth factors significantly affect the differentiation process, we investigated whether dual or single growth factor delivery could stimulate rMSC differentiation into the osteogenic lineage over a course of 10 days (Fig. 7). Real time PCR (RT-PCR) analysis of gene expression, including *ALP*, *OCN*, and *OPN*, were examined by qPCR. The gene expression of each study group was normalized to the control group. The results revealed a significant increase in the expression of the early osteogenic differentiation marker *ALP* in group BB. Although not significant, the BB group also showed a higher expression of the late osteogenic differentiation marker *OCN*. Levels of *OPN* expression, another late osteogenic differentiation marker, were significantly increased in the SVBB group.

3.6 Calcium deposition during differentiation

All osteogenic differentiated conditions for rMSC demonstrate the presence of insoluble calcium deposition, but mineralized nodules were not detected in the undifferentiated control group compared to the control medium

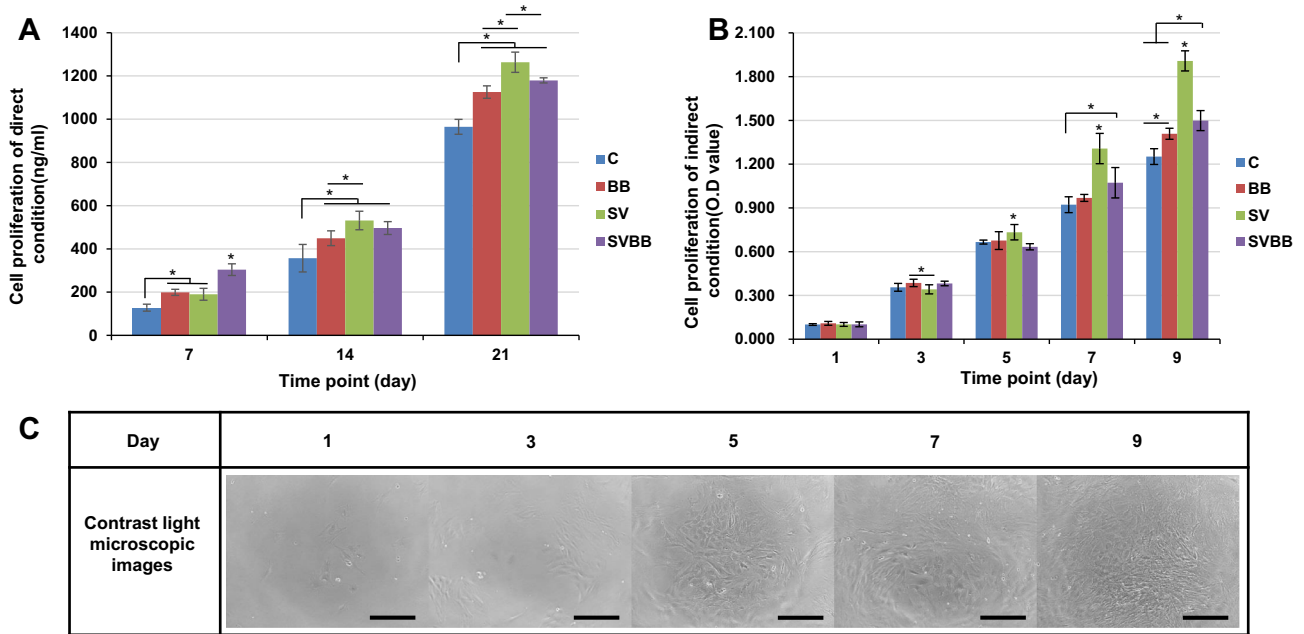


Fig. 5 A, B Proliferation after days 7, 14, and 21 under direct condition and days 1, 3, 5, 7, and 9 under indirect conditions. C: control; BB: big size microcarrier with BMP-2; SV: small size microcarrier with VEGF; SVBB: mixed microcarrier with BMP-2 and

VEGF. Asterisks represent samples presenting significantly higher cell growth ($* = p < 0.05$). C Contrast microscopy images obtained for cell culture under indirect culture conditions. Magnification $\times 100$, scale bar = 300 μm

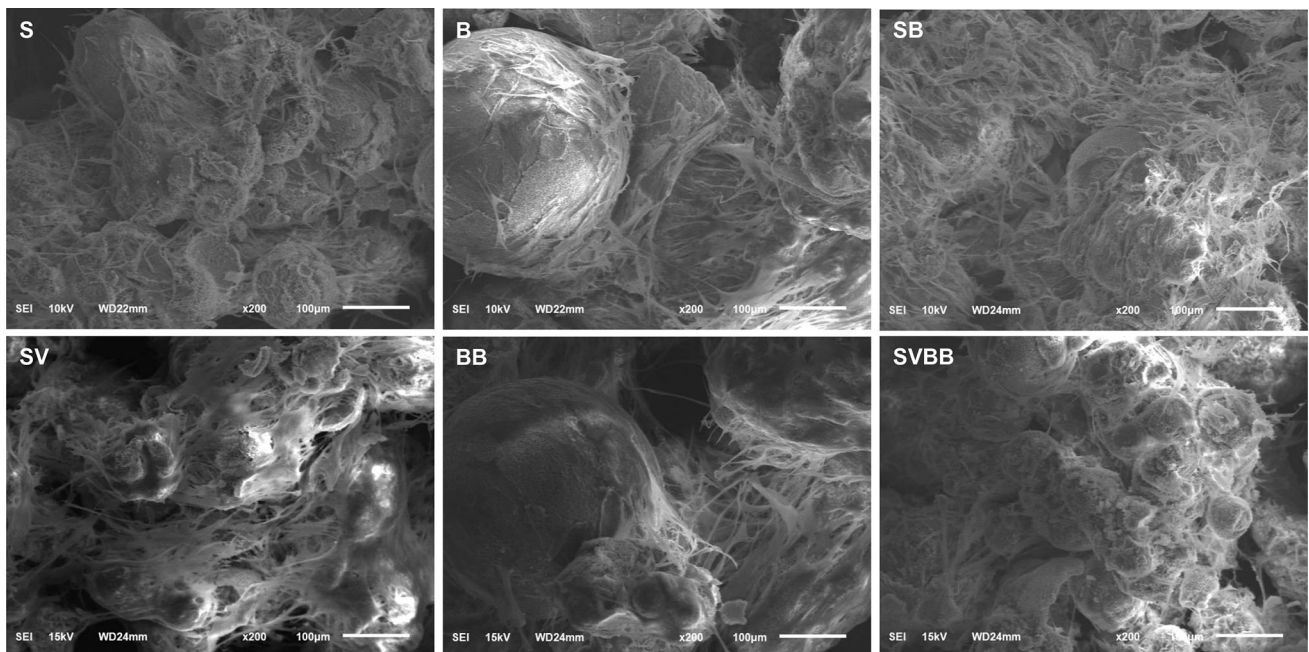


Fig. 6 SEM images for HA-MC at 2 weeks after osteogenic differentiation. Integration between HA-MCs by ECM can be observed at low magnifications. S: small size microcarrier; B: big

size microcarrier; SB: small and big size microcarrier; SV: small size microcarrier with VEGF; BB: big size microcarrier with BMP-2; SVBB: mixed microcarrier with BMP-2 and VEGF

during the study period (Fig. 8A). In all study groups, calcium deposition was first detected at day 10, and exhibited increasing positive staining until day 20. On day 10, the calcium deposition was significantly greater in MCs

with BMP-2 (BB & SVBB) as compared to other conditions. SVBB demonstrated higher calcium deposition than the BB group on day 15, but the deposition was similar on day 20 (Fig. 8B). SVBB demonstrated higher calcium

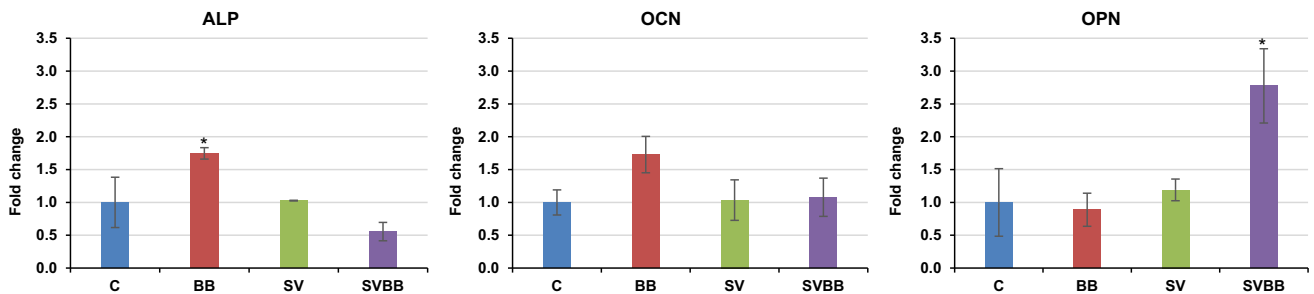


Fig. 7 Real time-PCR analysis of relative fold increase in ALP, OCN, and OPN expression in rMSCs. Asterisks represent samples presenting significantly higher gene expression compared to the other groups (* = $p < 0.05$). ALP alkaline phosphatase, OCN osteocalcin, OPN osteopontin

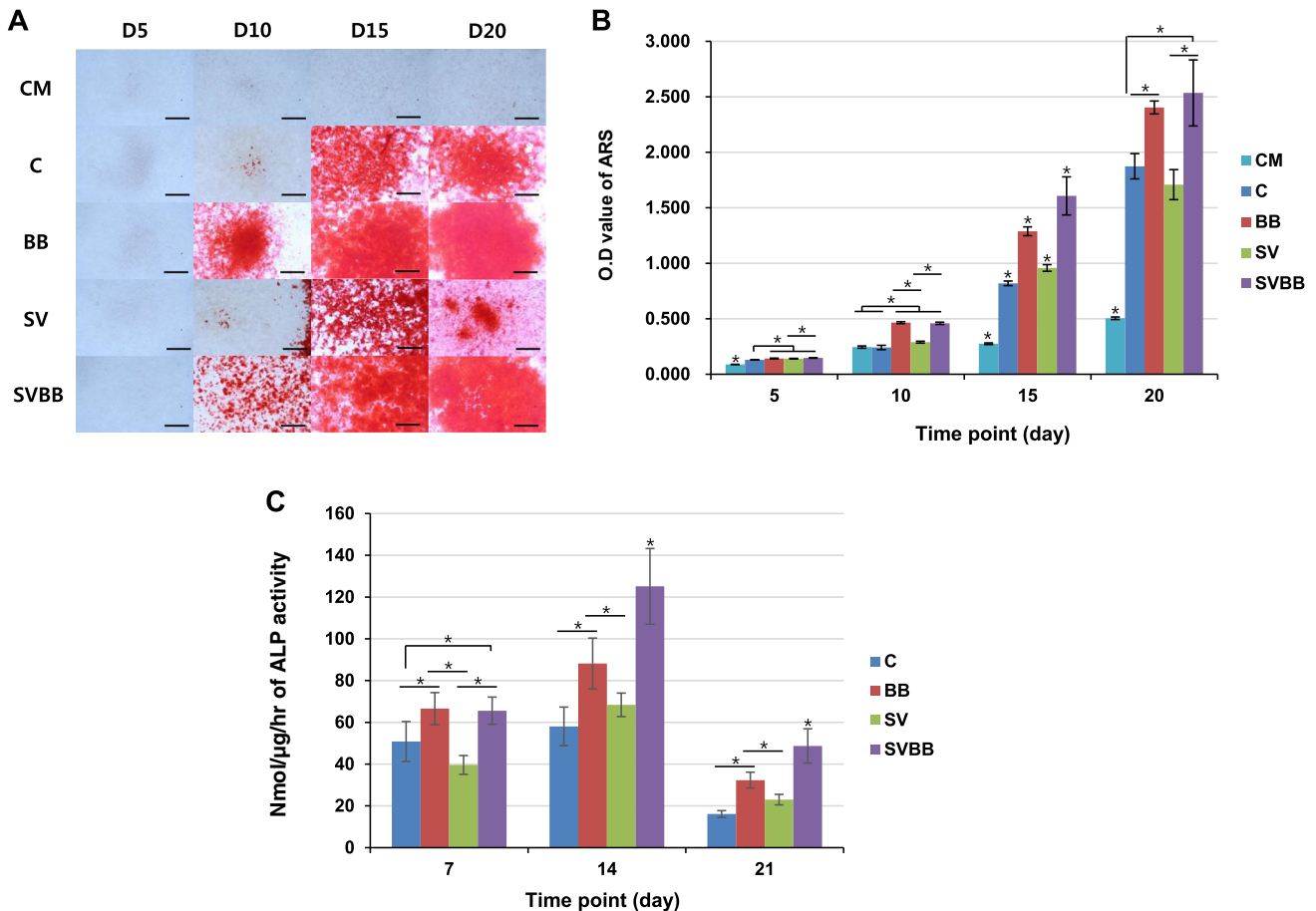


Fig. 8 Osteogenic differentiation of rMSCs on MCs. **A** Alizarin Red S (ARS) staining for insoluble calcium deposition was imaged at days 1, 3, 7, and 14. **B** For quantification of staining, ARS was extracted with 10% CPC and measured. Magnification $\times 100$, scale bar = 300 μm . **C** Measurement of the alkaline phosphatase activity in rMSCs at days 7, 14 and 21, subsequent to culturing with osteogenic medium.

Asterisks represent samples presenting significantly higher results compared to the other groups (* = $p < 0.05$). MCs microcarrier, rMSCs rat mesenchymal stem cells. CM: Conditioned medium; C: Control; BB: big size microcarrier with BMP-2; SV: small size microcarrier with VEGF; SVBB: mixed microcarrier with BMP-2 and VEGF

deposition than the BB group on day 15; the difference remained constant on day 20.

3.7 Alkaline phosphatase activity

We examined the effects of the MCs and growth factor loading on the ALP production at days 7, 14 and 21

subsequent to culturing rMSCs (Fig. 8C). ALP activity in osteogenic medium was enhanced on day 14 in all groups, compared to days 7 and 21. ALP activity measured over time revealed that the cells cultured on the BMP-2 incorporated MCs showed significantly higher level of ALP activity than others. In comparison with the BB group,

SVBB showed similar ALP production on day 7, but was comparatively significantly enhanced at days 14 and 21.

3.8 Biocompatibility and ectopic osteoinduction

The *in vivo* tissue responses of the MCs were first subcutaneously assessed in rats to analyze the osteoinductive potential of growth factor loaded MC (Fig. 9). Twelve weeks after implantation, residual scaffold materials remained within the fibrous capsules in all six study group MCs. Histological examination showed that all implanted MCs were biocompatible, and no immune reactions or tissue rejections were detected. Many fibroblastic cells encapsulated the MCs by collagenous tissue networks, and newly formed vessels were also shown within the fibrous capsule area for all groups. While growth factor not loaded and single growth factor loaded MCs did not induced ectopic bone formation, the SVBB group induced ectopic bone formation. However, bone apposition on the surface of the MC was not observed.

3.9 Bone regeneration in critical sized rat calvarial defect model

Based on the *in vitro* osteogenic differentiation and biocompatibility studies in subcutaneous tissues, we next examined the *in vivo* bone regeneration efficacy. To study this, only dual growth factor loaded MCs were considered.

MCs were implanted in a critical-sized bilateral parietal bone defect in rat calvaria with a diameter of 5 mm (Fig. 10A). For this purpose, we implanted SVBB (Fig. 10B). As a negative control, the defect was left empty, and SB alone was chosen as a second control group. All animals showed normal activity after 1 day of implantation, good healing response without adverse tissue reactions, and gained weight. The implanted site remained stable, and there was no evidence of inflammation in the harvested tissue.

Three-dimensional morphometric analysis of the μ CT images gave quantification of % bone volume after 8 weeks of implantation (Fig. 10C). When SB and SVBB groups were implanted in the defect, the values increased significantly. The volume percentage of new bone in defect area was 69.8 ± 6.0 in SVBB as compared to both control group EC (17.0 ± 2.9) and SB (58.4 ± 3.8) ($p < 0.05$). Significant increase in new bone formation was observed in the SVBB group, as compared to SB (Fig. 10D).

The histologic findings of H&E stained samples around the defect areas are presented in Fig. 11. All groups showed new bone ingrowth from the margin of the surgically created defects. However, the empty defect could not be healed spontaneously. Thin, loose connective tissues covered the defect area, and limited amount of newly formed bone could be seen along the edge of host bone. Compared to the empty control group, the other two groups

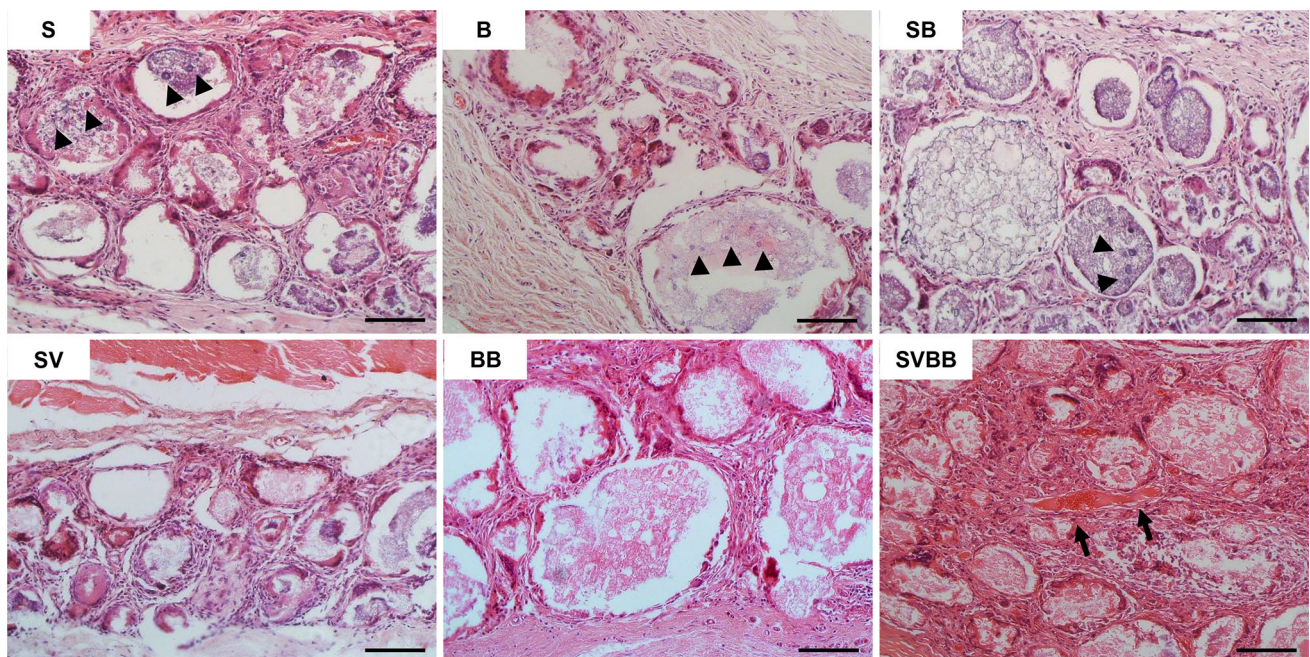


Fig. 9 Light microscope images of the biocompatibility and osteoinductive potential of dual growth factor loaded MCs subcutaneously implanted in rats. Histological sections showing the residual scaffold materials which remained within fibrous capsule without degradation. rMSCs extended into the MCs (arrow head). In group SVBB, some ectopic bone formation (arrow) was observed in the

space between MCs. H&E stain, magnification $\times 200$, scale bar = 100 μ m. S: small size microcarrier; B: big size microcarrier; SB: small and big size microcarrier; SV: small size microcarrier with VEGF; BB: big size microcarrier with BMP-2; SVBB: mixed microcarrier with BMP-2 and VEGF

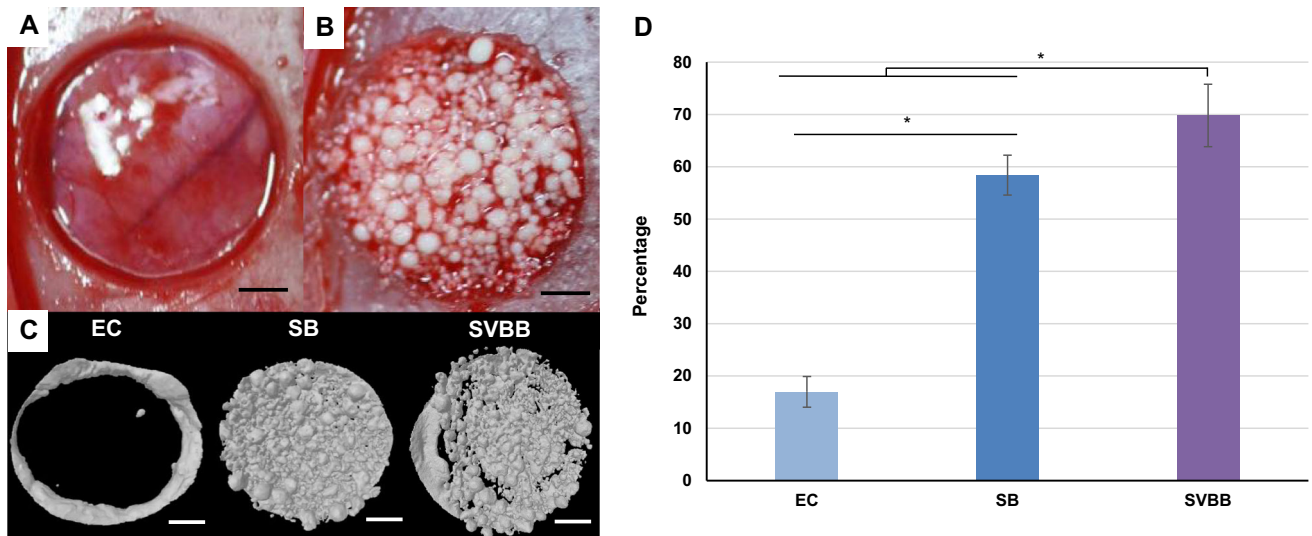
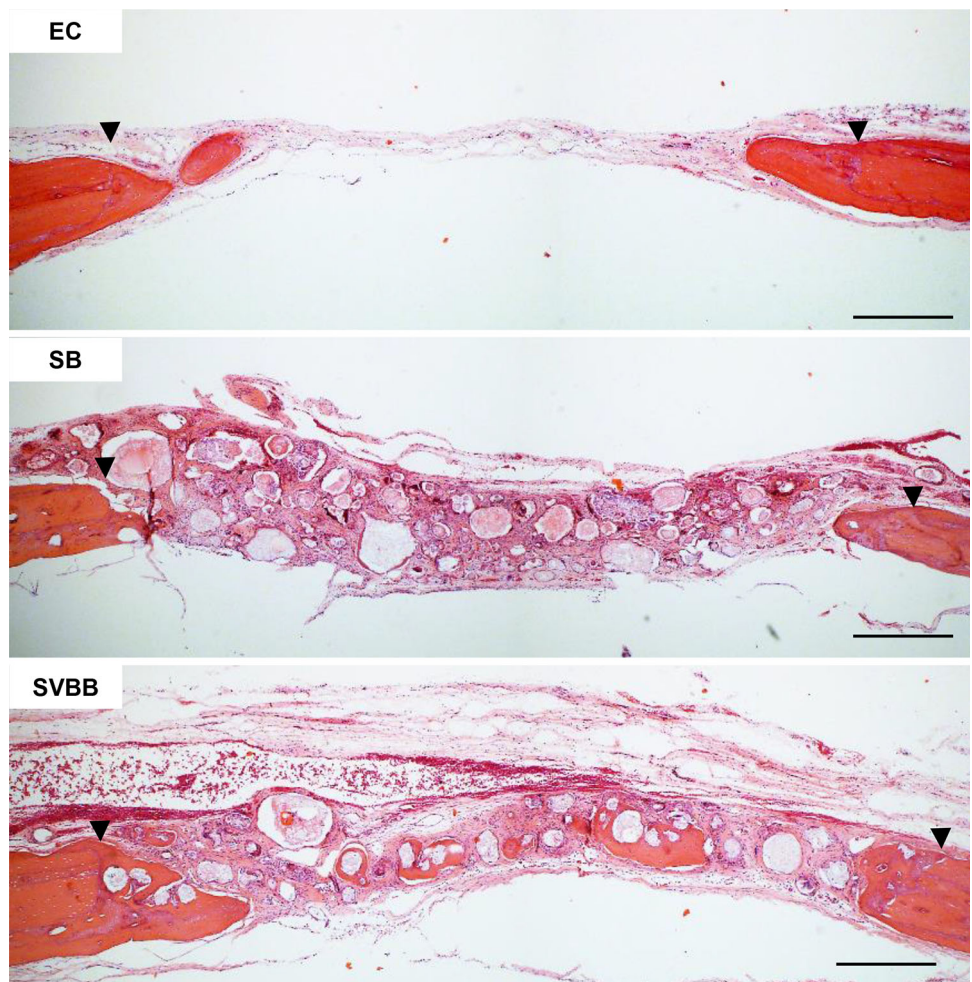


Fig. 10 Critical sized calvarial defect model in rats. **A** Macroscopic appearance of the standardized circular, full thickness bone defect. **B** Defect was either left empty as a negative control, or MCs were implanted. **C** Three-dimensional μ CT image of empty control (EC),

SV and SVBB group after 8 weeks. Bone formation outside the margins of the defect was found in all groups. **D** In the 8-week healing groups, there was statistical difference in % new bone formation between groups (* = $p < 0.05$). Scale bar = 1 mm

Fig. 11 Histologic findings of rat critical sized calvarial defects at 8 weeks. The arrowheads indicate the margin of the surgically created defect. New bone ingrowth was observed from the surgically created defect margin, and new bone was formed on the surface of the graft material both in the control (SB) and study group (SVBB). However, delivery of dual growth factors resulted in abundant new bone formation. Magnification $\times 200$, scale bar = 100 μ m. EC: empty control; SB: small and big size microcarrier; SVBB: mixed microcarrier with BMP-2 and VEGF



showed varying degrees of increased bone regeneration. In the SB group, better bone formation was demonstrated than in the empty control, but loose connective tissue was still found profoundly. In the SVBB group, abundant newly formed bone was observed on the surface of MC, and mature lamellar bone was identified in between the MCs. However, the particle size of MCs were not reduced.

4 Discussion

A variety of new materials have been introduced for bone regeneration, but research in tissue engineering and regenerative medicine continues, in an endeavor to find an optimal bone substitute. In the present study, spherical HA-MCs were obtained using oil emulsion of α -TCP paste, and two different osteogenic and angiogenic growth factors were successfully incorporated into the HA-MCs. These MCs, when used for bone tissue-engineering scaffold, showed a sustained release of the growth factors. *In vitro*, the MCs with double growth factors enhanced the osteogenic differentiation of rMSCs. The *in vivo* results demonstrated osteoinduction at the ectopic site with MCs, and enhanced bone regeneration in critical-sized rat calvarial defects model at 8 weeks post-implantation.

We studied calcium phosphate as a means of improving bioactivity and mechanical properties, and mimicking the extracellular matrix of bone. The scaffold composed of synthetic HA-MC showed tremendous potential in bone tissue engineering. The MC, composed of fully hydrolyzed HA from α -TCP, was obtained by an emulsion process. The spherical shape was revealed by SEM observations, as shown in Fig. 2. The effect of oil viscosity and rotation speed on MC mean size and sphericity for making HA-MCs from gelatin was a homogeneously incorporated α -TCP paste, and has been summarized previously [6]. Previous studies have shown that varying particle size of MCs can be obtained by controlling the solution concentration and production speed. MCs of various sizes, from tens of micrometers to hundreds of micrometers, have been manufactured and used for bone tissue engineering. For this study, two different MC sizes (100–200 μm and 300–500 μm) were chosen to compare bone regenerative characteristics for dual growth factor delivery. MCs of both sizes exhibited different porosity, which could be controlled by using them in combination (Fig. 2). Our future study plans include the effect of controlling porosity on bone formation, to help find the optimal bone tissue engineering effect by promoting the growth of newly generated tissues, and promoting the distribution of osteoprogenitor cells and endothelial cell migration into the matrix.

In this study, dual growth factors were incorporated into the MC. The concentration of growth factors used in this

experiment was determined according to previous studies, with BMP-2 corresponding to bone formation and VEGF corresponding to angiogenesis [15]. We observed burst release from the MCs for the first few hours, after which a sustained release of both growth factors was observed for up to 3 weeks. Since high-concentrations of growth factors can cause cytotoxicity, controlled release from such HA-Gel MCs is desirable for bone formation and angiogenesis. The addition of gelatin aims to control the drug release process of α -TCP [2]. Gelatin acts as a buffer system to inhibit burst release by interacting between growth factors and the matrix, slowing the drug release rate, and prolonging the total drug release time. Prolonged delivery of growth factors reduces inflammation due to excessive administration, promotes tissue formation, and stimulates the remodeling of newly formed bone tissue. Figure 3C, D show the rate at which the growth factors were released from the MC. The simultaneous release of two growth factors exhibited a reduced release pattern, wherein the reduction of VEGF was greater than that of BMP-2.

Bone marrow mesenchymal stem cells have the potential to differentiate into multilineage types such as osteoblasts, chondrocytes, and fibroblasts, and the differentiation into each cell type depends on the culture environment. rMSCs also show *in vitro* osteogenic differentiation under osteogenic media condition with dexamethasone [16] and *in vivo* bone formation in rat calvarial defect model [17]. It is important to establish a stabilized environment to enable bone tissue regeneration by promoting the activity of cell proliferation and differentiation *in vivo* or *in vitro* [10]. We investigated cell proliferation of MCs with dual growth factors with osteoconductive biomaterials, to provide a viable means of addressing the aforementioned regenerative conditions. Growth factor-loaded MCs showed a significant increase in cell growth, while VEGF single-loaded MCs showed the highest growth for rMSCs on both direct and indirect proliferation test. DNA quantification of direct proliferation test at day 7 showed that SVBB supports the highest proliferation of rMSCs compared to other MCs (Fig. 5A). However, no significant difference was detected between rMSCs proliferation on single growth factor loaded MCs which, in both cases, was significantly higher compared to control. However, this situation changed fundamentally between days 14 and 21, since VEGF alone supported better proliferation of rMSC compared to other groups. No significant differences were found between BB and SVBB during the study period, but SVBB supported maximum proliferation of rMSCs in the indirect test, as compared to other groups (Fig. 5B). VEGF is reported to have a dose-dependent proliferative effect, and we observed maximum proliferation at a concentration of hDPSCs of 40 ng/mL *in vitro* [18]. In the *in vivo* study, the possibility of dose-dependent potency of delivering VEGF

for bone regeneration has also been reported. In irradiated calvarial defect of 3.5 mm diameter, angiogenesis-enhanced bony bridging was similar to the sample non-irradiated by delivery of 3 μg of VEGF-containing scaffold [19]. Compared to BMP-2, VEGF provides a significant advantage for its proliferation by allowing expansion of undifferentiated rMSCs.

The surface properties of the scaffold provide physical cues to enable cell proliferation on the surface of the structure, which is influenced by several parameters including the culture and the seeding conditions of the cells [20]. Since an important application of MC could be its use as a cell delivery system for tissue engineering in *in vivo* applications, we investigated the possibility of rMSC to deposit mineralized ECM on MCs. Scanning Electron Microscopy (SEM) revealed that MCs with growth factors allowed cell growth on MC, and that the cells on the surface produced large amounts of ECM and aggregated them, as shown in Fig. 6. This also means that our HA-MCs exhibit excellent biocompatibility and osteoconductivity when used with gelatin. Compared to irregularly shaped microparticles, our spherical MCs can be applied through a minimally invasive route and provide additional mechanical support. Also, due to the predictable nature of implantation during filling, MCs can be used for bone defect filling applications in dentistry and orthopedics [21].

We further evaluated the regulation of osteogenic genes for osteogenic protein expression. The expression levels of osteogenesis-related genes, including *ALP*, *OCN*, and *OPN* in rMSCs cultured with MCs, were examined to determine the potential osteogenic effects of delivering two growth factors with two different size MCs. Growth factors affected the differentiation behavior of rMSCs, and mRNA expression tended to be up-regulated compared with control group. As a result, expressions of *ALP* were enhanced in MCs with single use BMP-2 on day 10. *ALP* is an early differentiation marker that indicates the state of differentiation. Activated *ALP* regulates the Wnt signaling pathway and plays an important role in mineralization of the ECM [22]. As a late indicator of osteoblast differentiation, *OCN* is a protein associated with hard tissue maturation [23]. The mRNA expression of *OCN* also increased under the same culture conditions, but the level was not significantly different between study groups. BMP-2 promotes osteoblast differentiation by increasing the expression of osteogenic genes through the activation of the TGF β receptor or BMP receptor signaling pathways [24]. The Smad protein is phosphorylated by BMP-2, binds to the receptor II on the cell membrane, and activates the receptor kinases. This complex is translocated to the nucleus to regulate the transcriptional activity of the target genes. The results of this experiment also revealed an upregulation in the *OPN* mRNA, the main non-collagenous protein of the

mineralized matrix, in the rMSCs cultured with dual growth factor. This indicates that SVBB plays an important role in promoting rMSC differentiation and osteogenesis, and that the growth factors released from the MCs maintained their biological activities effectively on the rMSCs, to induce osteogenic differentiation. VEGF binds to the tyrosine kinase receptors of VEGF receptor -1, -2 and -3 as an essential growth factor that induces and regulates angiogenesis by affecting endothelial cells. However, rMSCs were used in this experiment, and no genes associated with VEGF were evaluated.

Consistent with gene expression studies, we further evaluated the common markers in osteogenesis research: *ARS* for mineralized nodule formation and *ALP* activity (Fig. 8). We found that the rMSCs treated with SVBB exhibited significantly enhanced *ALP* activity when compared to other study groups. BMP-2 loaded MCs showed higher *ALP* activity over the entire experimental period, and peak *ALP* activity of rMSC was observed at day 14 in SVBB compared to other groups. This data suggests that the biological activity of VEGF and BMP2 released from SVBB promotes the induction of rMSC osteogenic differentiation of rMSCs, and synergistically enhanced mineralization [9]. Although VEGF is an essential regulator of extracellular matrix remodeling and angiogenesis, it inhibits MSC differentiation; hence, SV exhibits the lowest *ALP* activity on day 7. We also observed increased mineralization in rMSC when BMP-2 was involved. BMP-2 is involved in the initiation of mineralization, but VEGF did not induce mineralization in human dental pulp stem cells or human adipose-derived stem cells [25]. The positive alizarin red staining results were similar in both BB and SVBB, suggesting that mineralization by BMP-2 is similar to the effect seen in BMP-2 and VEGF combined. Compared to other MCs, mineralization level is significantly increased in SVBB after day 15. This may be due to the combined effects of VEGF and BMP-2, in which VEGF acts in the early proliferation stage and BMP-2 acts in the late differentiation stage in osteogenesis differentiation of MSCs [26]. Low levels of mineralization of SV may be associated with VEGF, which inhibits differentiation at later stages but promotes the proliferation of rMSC at an early stage [9]. SVBB increased the expression of *ALP*, the major enzyme involved in ECM maturation, and showed calcium deposition in the ECM. This indicates that the differentiation and maturation of rMSCs to osteoblasts induced by BMP2 and VEGF can be combined [9]. These *in vitro* results suggest the possibility of delivering dual growth factors using MCs as bone tissue engineering constructs.

Since BMP-2 and VEGF were released from MCs in controlled profiles and the released growth factors were effective in rMSCs, we further investigated whether these MCs could induce osteogenic responses *in vivo*. The

ectopic bone formation, a critical parameter of osteoinduction for comparing MCs, was confirmed in rat subcutaneous pouch after 8 weeks of implantation. The controlled delivery of bone regenerative factors through the carrier system facilitates infiltration and proliferation of cells into the target site by local delivery of certain regenerative agents, facilitates the repair of defects by biodegradation, and replaces them with new regenerated tissue [5]. Unlike other MCs, despite the burst release characteristics, SVBB induced ectopic bone formation (Fig. 9). No significant effect was observed in the use of VEGF or BMP-2 alone in ectopic bone formation. Of the various biomaterials, HA-gelatin composite MCs are reportedly superior to stem cell differentiation and osteoinduction *in vivo*, and the VEGF-BMP-2 combination was seen to enhance the angiogenic and osteogenic effects [27, 28]. Our MCs provide ectopic osteoinductive ability during spontaneous bone formation while maintaining the BMP-2 bioactivity over a longer period of time, and VEGF supported the bone tissue indirectly by increasing the vascular network and vascular permeability. VEGF-mediated vascular changes and chemoattractant activity can lead to efficient ectopic bone formation induced by BMP-2 by enhancing the local blood flow and improving local cell recruitment of osteoprogenitors.

We compared the osteogenic effect of dual growth factor incorporated MCs using not only ectopic implantation, but also critical sized calvarial defect models in rat. For this purpose, two study groups were selected from the previous experiments, namely SB and SVBB. To evaluate the ability of HA incorporated with dual growth factors to regenerate bones, two groups of MCs were implanted in bilateral cranial defects into the bilateral calvarial defects in rat, with a critical-size diameter of 5 mm. The critical-size defect (CSD), the smallest diameter intraosseous defect that does not heal spontaneously, was used as a model to evaluate bone healing. Without treatment, bone defects are filled with fibrous connective tissue, rather than regenerated bone, due to the limited ability to regenerate due to poor blood supply and a relative deficiency of bone marrow. As a result of implantation of SB and SVBB into a rat calvarial defect by μ CT and subsequent histological assessments, SVBB showed better bone regeneration and angiogenesis than SB. The precise quantified result of new bone growth in defects was defined by 3D image analysis using μ CT (Fig. 10). The CSD in rat calvaria is well suited for placing particulate materials, and because it has a thin structure, high-resolution radiographic image analysis could easily assess bone healing by the implanted material. The total amount of bone, including newly regenerated bone and implanted MCs, was observed to have increased to some extent. However, new bone formation was significantly greater in the SVBB group after 8 weeks than in

the SB and empty control groups, and the difference in osteogenic potential between SVBB and SB was clearly apparent. Although the volume of the new bone was lower on SB, the MCs alone also showed better osteogenic potential than the empty control group. Bone apposition was highest in SVBB followed by SB, and significantly less bone was observed in empty defects (Fig. 10).

Histological analysis showed that degradation of the scaffold was not evident, and MCs were present in the bone defect after 8 weeks healing periods. The MCs were covered with new bones, but the resorption of the MCs was not clear. No replacement of MCs with newly formed bones was observed, as the generated bone was stacked to the surface of the MCs. This shows that biodegradation did not promote the release of growth factors, similar to the *in vitro* release conditions. These results indicate that dual growth factors induce rapid bone formation and remodeling at an earlier stage. As shown in Fig. 11, newly formed bone appeared to begin from the surgically created defect margin, and woven bone covered the bone graft materials. This may be due to the osteoconductive role of the released growth factor from the MCs [14]. A large amount of osteoids undergoing calcification process are present in new bone tissue near and adjacent to the scaffold. Both chemical properties of the graft materials and biological properties of the growth factors may influence the *in vivo* osteogenic potential, and this is consistent with findings of a previous study [29]. Wenjie Zhang et al. reported that BMP-2 enhanced the recruitment of circulating or surrounding MSCs to the implantation sites, and promoted bone regeneration in addition to osteoinductive effects on local MSCs [30]. Improved regeneration of critical size bone defects is due to the effective enhancement of angiogenesis essential for bone regeneration by VEGF delivered by MCs [27]. VEGF can be used in combination with osteoinductive factors to improve cell recruitment and lead to more efficient bone regeneration [27]. According to Song et al., the specific role of VEGF in bone healing has not yet been elucidated, but an interaction with other factors such as BMP-2 should lead to a greater effect of bone regeneration [31]. These results suggest that the locally released growth factors from MCs in the bone defects effectively promote new bone formation by acting on the osteogenic and angiogenic processes of the stem cells present in the surrounding tissues. The bone regeneration was enhanced by the synergistically coordinated osteoconduction effects of HA, osteogenic effects of BMP-2, angiogenic effects of VEGF, and rMSCs recruitment by both growth factors. Better bone regeneration was possible by the interaction between osteogenesis and angiogenesis. However, these results cannot be interpreted that more graft materials were substituted with new bone. We deduce that the bone graft materials coated with growth factors

showed better osteoconductive potential than bone graft materials alone.

In the present study, an HA microcarrier was constructed by a combination of α -TCP and gelatin emulsification using the water-in-oil emulsion method. Furthermore, both osteogenic and angiogenic growth factors were successfully incorporated into small and big size HA-MCs, and these MCs showed osteogenic and angiogenic activities concurrently. The small and big size combination and stand-alone MCs represented a sustained release of VEGF and BMP-2 for 21 days. Released growth factors showed increased osteoblast differentiation, exhibited by enhanced ECM formation, osteogenic genes, and accelerated mineralization. More importantly, combination of MCs induced ectopic bone formation and enhanced the bone regeneration. These findings are considered a promising therapeutic application of MCs with double growth factors, as a therapeutically relevant tissue engineered construct for bone regeneration by simultaneously enhancing osteogenesis and angiogenesis.

Acknowledgements This research was supported by Basic Science Research Program through the National Research Foundation of Korea (NRF) funded by the Ministry of Education (Grant No: NRF-2017R1D1A1B03035962) and Korea University Grant (Grant No: k1710621).

Compliance with ethical standards

Conflict of interest The authors declare no potential conflicts of interest with respect to the authorship and/or publication of this article.

Ethical statements Animal cell primary culture and the protocol of housing, care and experimental procedure were approved by the Korea University Institutional Animal Care and Use Committee (Korea-2016-0111), Republic of Korea.

References

- Mourão CF, Valiense H, Melo ER, Mourão NB, Maia MD. Obtention of injectable platelets rich-fibrin (i-PRF) and its polymerization with bone graft: technical note. *Rev Col Bras Cir.* 2015;42:421–3.
- Yu WL, Sun TW, Qi C, Zhao HK, Ding ZY, Zhang ZW, et al. Enhanced osteogenesis and angiogenesis by mesoporous hydroxyapatite microspheres-derived simvastatin sustained release system for superior bone regeneration. *Sci Rep.* 2017;7:44129.
- Dickson KF, Katzman S, Paiement G. The importance of the blood supply in the healing of tibial fractures. *Contemp Orthop.* 1995;30:489–93.
- Stegen S, van Gastel N, Carmeliet G. Bringing new life to damaged bone: the importance of angiogenesis in bone repair and regeneration. *Bone.* 2015;70:19–27.
- Vo TN, Kasper FK, Mikos AG. Strategies for controlled delivery of growth factors and cells for bone regeneration. *Adv Drug Deliv Rev.* 2012;64:1292–309.
- Perez RA, Del Valle S, Altankov G, Ginebra MP. Porous hydroxyapatite and gelatin/hydroxyapatite microspheres obtained by calcium phosphate cement emulsion. *J Biomed Mater Res B Appl Biomater.* 2011;97:156–66.
- Choi H, Park NJ, Jamiyandorj O, Choi KH, Hong MH, Oh S, et al. Improvement of osteogenic potential of biphasic calcium phosphate bone substitute coated with two concentrations of expressed recombinant human bone morphogenetic protein 2. *J Periodontol Implant Sci.* 2012;42:119–26.
- Park JH, Pérez RA, Jin GZ, Choi SJ, Kim HW, Wall IB. Microcarriers designed for cell culture and tissue engineering of bone. *Tissue Eng Part B Rev.* 2013;19:172–90.
- Barati D, Shariati SRP, Moeinzadeh S, Melero-Martin JM, Khademhosseini A, Jabbari E. Spatiotemporal release of BMP-2 and VEGF enhances osteogenic and vasculogenic differentiation of human mesenchymal stem cells and endothelial colony-forming cells co-encapsulated in a patterned hydrogel. *J Control Release.* 2016;223:126–36.
- Lin Z, Wang JS, Lin L, Zhang J, Liu Y, Shuai M, et al. Effects of BMP2 and VEGF165 on the osteogenic differentiation of rat bone marrow-derived mesenchymal stem cells. *Exp Ther Med.* 2014;7:625–9.
- Walker DH, Wright NM. Bone morphogenetic proteins and spinal fusion. *Neurosurg Focus.* 2002;13:e3.
- Kim JW, Choi KH, Yun JH, Jung UW, Kim CS, Choi SH, et al. Bone formation of block and particulated biphasic calcium phosphate lyophilized with Escherichia coli-derived recombinant human bone morphogenetic protein 2 in rat calvarial defects. *Oral Surg Oral Med Oral Pathol Oral Radiol Endod.* 2011;112:298–306.
- Park JC, So SS, Jung IH, Yun JH, Choi SH, Cho KS, et al. Induction of bone formation by Escherichia coli-expressed recombinant human bone morphogenetic protein-2 using block-type macroporous biphasic calcium phosphate in orthotopic and ectopic rat models. *J Periodontol Res.* 2011;46:682–90.
- Kim JH, Kang MS, Eltohamy M, Kim TH, Kim HW. Dynamic mechanical and nanofibrous topological combinatory cues designed for periodontal ligament engineering. *PLoS One.* 2016;11:e0149967.
- Kim JH, Kim TH, Jin GZ, Park JH, Yun YR, Jang JH, et al. Mineralized poly(lactic acid) scaffolds loading vascular endothelial growth factor and the in vivo performance in rat subcutaneous model. *J Biomed Mater Res A.* 2013;101:1447–55.
- Jin GZ, Kim JH, Park JH, Choi SJ, Kim HW, Wall I. Performance of evacuated calcium phosphate microcarriers loaded with mesenchymal stem cells within a rat calvarium defect. *J Mater Sci Mater Med.* 2012;23:1739–48.
- Kim TH, Singh RK, Kang MS, Kim JH, Kim HW. Gene delivery nanocarriers of bioactive glass with unique potential to load BMP2 plasmid DNA and to internalize into mesenchymal stem cells for osteogenesis and bone regeneration. *Nanoscale.* 2016;8:8300–11.
- Aksel H, Huang GT. Combined effects of vascular endothelial growth factor and bone morphogenetic protein 2 on odonto/osteogenic differentiation of human dental pulp stem cells in vitro. *J Endod.* 2017;43:930–5.
- Kaigler D, Wang Z, Horger K, Mooney DJ, Krebsbach PH. VEGF scaffolds enhance angiogenesis and bone regeneration in irradiated osseous defects. *J Bone Min Res.* 2006;21:735–44.
- Confalonieri D, La Marca M, van Dongen EMWM, Walles H, Ehlicke F. An injectable recombinant collagen I peptide-based macroporous microcarrier allows superior expansion of C2C12 and human bone marrow-derived mesenchymal stromal cells and

- supports deposition of mineralized matrix. *Tissue Eng Part A*. 2017;23:946–57.
21. Bohner M, Tadier S, van Garderen N, de Gasparo A, Döbelin N, Baroud G. Synthesis of spherical calcium phosphate particles for dental and orthopedic applications. *Biomater*. 2013;3:e25103.
 22. Zhu B, Liu W, Liu Y, Zhao X, Zhang H, Luo Z, et al. Jawbone microenvironment promotes periodontium regeneration by regulating the function of periodontal ligament stem cells. *Sci Rep*. 2017;7:40088.
 23. Kim JH, Ko SY, Lee JH, Kim DH, Yun JH. Evaluation of the periodontal regenerative properties of patterned human periodontal ligament stem cell sheets. *J Periodontal Implant Sci*. 2017;47:402–15.
 24. Bae SJ, Kim HJ, Won HY, Min YK, Hwang ES. Acceleration of osteoblast differentiation by a novel osteogenic compound, DMP-PYT, through activation of both the BMP and Wnt pathways. *Sci Rep*. 2017;7:8455.
 25. Behr B, Tang C, Germann G, Longaker MT, Quarto N. Locally applied vascular endothelial growth factor a increases the osteogenic healing capacity of human adipose-derived stem cells by promoting osteogenic and endothelial differentiation. *Stem Cells*. 2011;29:286–96.
 26. Bai Y, Li P, Yin G, Huang Z, Liao X, Chen X, et al. BMP-2, VEGF and bFGF synergistically promote the osteogenic differentiation of rat bone marrow-derived mesenchymal stem cells. *Biotechnol Lett*. 2013;35:301–8.
 27. Kempen DH, Lu L, Heijink A, Hefferan TE, Creemers LB, Maran A, et al. Effect of local sequential VEGF and BMP-2 delivery on ectopic and orthotopic bone regeneration. *Biomaterials*. 2009;30:2816–25.
 28. Perez RA, Riccardi K, Altankov G, Ginebra MP. Dynamic cell culture on calcium phosphate microcarriers for bone tissue engineering applications. *J Tissue Eng*. 2014;5:2041731414543965.
 29. Hernández A, Reyes R, Sánchez E, Rodríguez-Évora M, Delgado A, Évora C. In vivo osteogenic response to different ratios of BMP-2 and VEGF released from a biodegradable porous system. *J Biomed Mater Res A*. 2012;100:2382–91.
 30. Zhang W, Zhu C, Wu Y, Ye D, Wang S, Zou D, et al. VEGF and BMP-2 promote bone regeneration by facilitating bone marrow stem cell homing and differentiation. *Eur Cells Mater*. 2014;27:1–11.
 31. Song X, Liu S, Qu X, Hu Y, Zhang X, Wang T, et al. BMP2 and VEGF promote angiogenesis but retard terminal differentiation of osteoblasts in bone regeneration by up-regulating Id1. *Acta Biochim Biophys Sin (Shanghai)*. 2011;43:796–804.

Publisher's Note Springer Nature remains neutral with regard to jurisdictional claims in published maps and institutional affiliations.